machines

Article

Vibration Propagation Characteristics of Micro-Milling Tools

Binghui Jia

School of Mechanical Engineering, Nanjing Institute of Technology, Nanjing 211167, China; bhjia@njit.edu.cn

Abstract: Micro-milling tools are usually used for the 3D precision processing of micro metal parts under ultra-high speed. However, due to the structural characteristics of small scale, variable cross-section, and weak stiffness, the vibration of micro-milling tools is weak and easily mutates, which can potential cause great harm to the stability and machining accuracy of machine tools. To reveal the transfer law of micro-milling tool vibration, guiding the method selection of tool vibration measurement and providing new means for mechanical model verification; firstly, the vibration mechanics model and vibration transfer matrix of the micro-milling tool were established. The vibration propagation characteristics of the micro-milling tool were analysed in contrast with the time domain and frequency domain, taking two representative micro-milling tools, Tool A and Tool B, as examples which with different cross-sections and structural parameters. Secondly, a micro-milling tool vibration measurement experimental system was set up and a sensor array with four optical fibre displacement sensors was used to obtain the vibration displacements at different positions of the tool under pulse and start-stop excitation. Finally, the results show the following: for Tool A, the max vibration displacement of the measurement of point 1 is about 3.5 times of measurement point 2 but near 18 times the measurement of point 3; meanwhile, compared with measurement point 1, the 16.8 kHz signal disappeared in measurement point 2, measurement point 3 and measurement point 4. However, for Tool B, the max vibration displacement of measurement point 1 is about 11.24 times the measurement of point 2; in contrast, the signal strength of the measurement of point 3 and point 4 is too weak to compare and analyse, although there are three resonant frequencies (10.2 kHz, 17.6 kHz, and 26.7 Hz) of Tool B based on the signal of measurement point 1, the 26.7 kHz signal disappeared in measurement point 2. The vibration amplitude of the tool tip decreases rapidly in the process of tool transfer, a bigger ratio cross-section with bigger attenuation of vibration amplitude and smaller size will aggravate this process. This study provides a reference for the selection of measuring points of micro-milling tool vibration displacement.

Keywords: micro-milling tool; vibration propagation; non-uniform cross-section; measurement

Citation: Jia, B. Vibration Propagation Characteristics of Micro-Milling Tools. *Machines* **2022**, *10*, 946. https://doi.org/10.3390/machines10100946

Academic Editor: Dimitrios Giagopoulos

Received: 15 September 2022
Accepted: 17 October 2022
Published: 18 October 2022

1. Introduction

Micro-milling is an important advanced manufacturing technology in the field of micromachining [1]. It is the technology from electric processing to non-electric processing, silicon micro-processing to non-silicon micro-processing, and two-dimensional processing to three-dimensional processing. It has become an effective way to process small, complex 3D structural parts [2,3]. With the gradual expansion of processing object and application range, it is being used for more high-quality parts processing, such as in the aerospace, precision instruments, biomedical, automotive, and microelectronics fields. However, due to the huge variable cross-section, weak stiffness, and greatly reduced scale of the micro-milling tool, the processing mechanism of micro-milling is significantly different from traditional milling. It presents three typical characteristics [4,5]: ① The strains and positions of the micro-milling tools are different under different kinds and directions of complex impact forces. ② As the processing size is reduced to micron and sub-micron scales, the cutting depth of the micro-milling tool is often less than the grain diameter of the material, and many physical phenomena and basic laws in the macro world are no longer fully applicable to the micro world. The micro surface force, friction force, and heat transfer mode in the micro world play a major role. At the same time, the discontinuity and heterogeneity of materials also cause complex nonlinear cutting force fluctuation at high frequencies. ③ The ultra-high-speed spindle radial runout under the centrifugal force is amplified, caused by the inevitable installation errors of tool installation tilt and eccentricity. These extremely complex factors affect the variation of the cutting force and cutting vibration signal together, meanwhile forcing micro-milling tools to present a variety of motion patterns [6]. In order to predict and suppress micro-milling tool vibration, two methods are commonly used: the vibration mechanical model and vibration measurement.

The vibration mechanical model is an important way to understand the generation and development of the vibration of micro-milling tools. Therefore, considering the scale effect and other factors, early researchers have performed many studies based on the conventional milling processing law [2]. Huaizhong Li [7] measured the vibration signals using accelerometers in the machining process and presented the characteristics related to chatter occurrence in micro-milling operations. Considering tool runout, the dynamic displacement of the tool, the workpiece contour left by previous tool paths, and the wavy surface, Wangqun Chen [8] established an uncut chip thickness model. A deeper understanding of micro-milling processing rules, tool runout, the relative motion between the tool and the work piece, and the instantaneous uncut thickness change with the tool vibration were taken into account one after the other. David, C. [9] evaluated the effect of runout on tool vibration based on experimental analysis under various cutting process parameters, such as the cutting speed, feed rate, and axial cutting depth. In order to improve the understanding of the connection between the dynamic cutting process and abnormal tool response, K.B. Mustapha [10] presented a hybrid analytical model. The model combination of discrete and distributed structural elements was used for estimating the transverse response of the micro end mill. Based on the strain gradient elasticity theory and the Hamiltonian principle, Qinghua Song [11] established a micro-milling tool model considering the shear deformation and rotational inertia of the micro-milling tool. Additionally, the static and dynamic characteristics of the micro-milling tool under different tool diameters and different slenderness ratios were studied. However, due to the high precision requirements of micro-milling, researchers have to take more complex factors that may cause micro-milling vibration into account to obtain a more accurate tool vibration prediction model. Xiaohong Lu [12] established a micro-milling surface roughness model considering the tool vibration. The model studies the relationship between tool vibration and machined surface roughness. Then, another rotary Timoshenko beam model of the micro-milling spindle system was established, and the effects of spindle centrifugal force and gyro effect on the frequency response characteristics of the tool system and its stability region were studied [13]. In summary, vibration, as an important factor affecting the stability of ultra-high speed precision micro-milling, is affected by a variety of complex factors, such as machine tool structure, material properties, processing parameters, tool runout, etc. Therefore, establishing a comprehensive model considering all factors to express the relationship between vibration and system parameters is very complex. Furthermore, the above research mostly focuses on the effects of tool vibration on work piece processing quality and lacks analysis of the tool vibration itself. Sensors and measurement techniques are an important complement to those research approaches.

Sensors and measurement techniques are other means for understanding tool vibration. Scholars use laser displacement sensors [14,15], acoustic emission sensors [11], three-dimensional cutting force sensors [16,17], acceleration sensors [2], or integrate the above-mentioned sensors [18–20] to obtain signals of micro-milling vibration displacement, sound, cutting force, acceleration, current, and so on. They are used for monitoring, fault diagnosis, and the performance evaluation of machine tool or tool state, realizing function failure judgment, and processing the ability evaluation of machine tools. For example, Xiaohong Lu [14] developed a micro-milling vibration measurement system based on a laser displacement sensor. The system can be extended to measure vibration in three directions simultaneously, which provides an experimental condition for the research of vibration suppression in micro-milling. Tsai, N.C. [15], proposed a real-time flutter detection method based on acoustic emission and applied the acoustic feedback signal analysis and processing to control the spindle motor speed. In order to identify the chatter and tool wear simultaneously, Runqiong Wang [17] proposed a multi-condition identification method based on sensor fusion by fusing sound, acceleration, and cutting bending moment signals data. Polli, M.L. [20], comprehensively utilized force sensors, acoustic emission sensors, and acceleration sensors to obtain micro-milling processing signals. Nevertheless, these studies are more interested in the measurement itself. It is assumed that the measurement method obtained accurate tool vibration information but the vibration transfer law and vibration dissipation were not paid much attention.

Thus, the above research studied the vibration mechanical model, measurement method, and vibration prediction model of micro-milling tools from different angles. They undoubtedly deepen the general understanding of micro-milling and improve machining stability and accuracy. However, some questions currently remained unanswered; for instance, which vibration signals are reliable? What data are available in terms of flutter prediction? How should suitable measurement points to verify the model be selected. Furthermore, research on the vibration transfer characteristics of micro-milling tools is not enough, as their small size, large variable cross-section, and weak rigidity characteristics make them significantly different from traditional milling tools. Hence, this paper focuses on the above questions and tries to explore the vibration transfer law of micro-milling tools. Although there is much research on the vibration transfer characteristics of structures with variable cross-sections, they mainly focus on large structures [21–23]. From the micro-milling tool vibration point of view, research is not sufficient, as micro-tools are of very small size (from the submicron to millimetre scale), with larger variable cross-sections (in a very short distances, the cross-sectional area of the tool tip and the tool bar differs by a hundred times) and weak rigidity characteristics. This is a different perspective and also the novelty of this paper compared with the existing research on micro-milling tool vibration.

In order to answer the questions mentioned above, this paper is organized into three sections. The first focuses on the vibration propagation model of the micro-milling tool. The two-dimensional vibration mechanics model and the vibration transfer matrix of the micro-milling tool are established. The second section is centred on the vibration characteristics analysis of the micro-milling tool. Two representative micro-milling tools are taken as an example. Their vibration propagation characteristics in the time domain and frequency domain are analysed, respectively. To verify the above model and simulation results, a micro-milling tool vibration measurement experimental system was set up, and a sensor array with four optical fibre displacement sensors was used to obtain the vibration displacements at different positions of the tool under pulse excitation. The third section presents the measurement results of two micro-milling tools in the machine start–stop process. The influence of the tool section area on vibration transmission is discussed. The three sections aim to explore the vibration transfer characteristics of micro-cutting tools in detail.

2. Vibration Propagation Modeling in the Micro End Milling Process

2.1. Vibration Model of the Micro-Milling Tool

Generally, there are three parts to the cutting force in the milling process: the static cutting force, the elastic and plastic deformation force that used to overcome the resistances of material processing, and the friction between the cutter and the machined surface and chip. However, the scale effect plays a major role in the micro-milling process due to the significant reduction of tool geometry [24], and the method is no longer appropriate for micro-milling tool force analysis which is based on traditional macro-milling. In order to simplify the analysis, the material removal process by cutting tool is regarded as a large ball (tool tip) impinging on a small ball (metal crystal cluster), as Figure 1 shows. Considering the micro-milling cutting mode with the characteristics of high speeds and an interrupted cut, there are two main parts of the force in micro-milling process: one is the force by which the knife tip breaks the interaction between metallic crystals, which can be obtained by test molecular dynamics (MD) simulations [25], denoted as F_t; the other is the force that alters the motion of clusters of metal crystals being cut according to the mass of the chip, denoted as F_c. Based on above hypothesis, the micro end milling process can be presented as Equation (1); it is a two degrees of freedom system [26].

$$\begin{cases} m_u\ddot{u}(x,t) + c_u\dot{u}(x,t) + k_u u(x,t) = F_u \\ m_w\ddot{w}(x,t) + c_w\dot{w}(x,t) + k_w w(x,t) = F_w \end{cases} \tag{1}$$

where m_u, m_w, c_u, c_w, k_u, k_w are the mass, damping, and stiffness in the feed (y) and (z) direction.

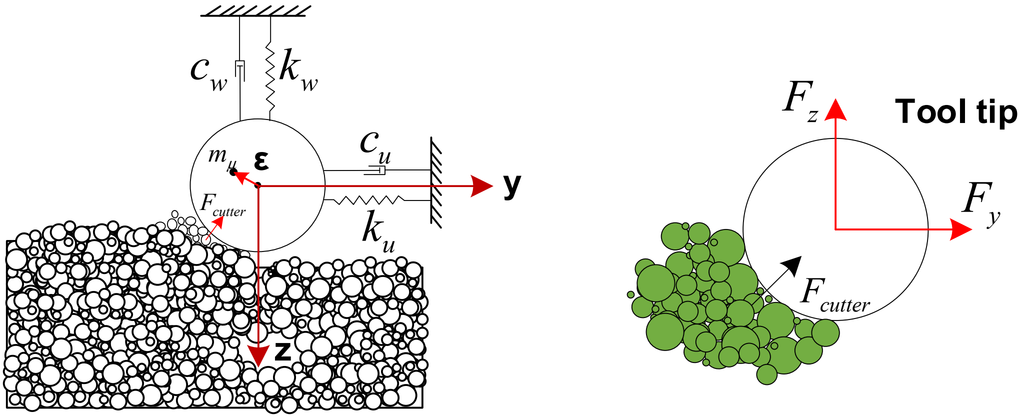

Figure 1. Two-degree freedom system of micro end milling operations.

F_u and F_w are external excitations which contain two parts: mass unbalance caused by the run-out and tool geometry errors brought about by tool wear or machining intolerance and cutting force, so:

$$\begin{bmatrix} F_u & F_w \end{bmatrix} = \boldsymbol{F_{unbalance}} + \boldsymbol{F_{cutter}} \tag{2}$$

The mass unbalance caused by the run-out of the tool can be denoted as "centrifugal force", and its associate kinetic energy can be approximated as:

$$F_{unbalance} = \begin{bmatrix} m_\mu\Omega^2\varepsilon u(x_u,t)\sin(\Omega t) & m_\mu\Omega^2\varepsilon w(x_u,t)\sin(\Omega t) \end{bmatrix} \tag{3}$$

$$F_{cutter} = F_t + F_c \tag{4}$$

The machine tool spindle speed is denoted by Ω and the cutting depth by t_c. As the cutting width depends on the tool tip size, the tip radius is denoted by r_{tip} and the material removal rate factor is denoted by t_α (depending on how fast the material is removed according to the speed). Based on the law of conservation of energy, F_c can be calculated by Equation (5).

$$F_c = 2\rho t_c {r_{tip}}^{\frac{5}{2}} \frac{\sqrt{2\Omega}}{t_\alpha} \tag{5}$$

$$\begin{cases} F_u = m_\mu\Omega^2\varepsilon u(x_u,t)\sin(\Omega t) + F_{cutter}\cos(\Omega t) \\ F_w = m_\mu\Omega^2\varepsilon w(x_u,t)\cos(\Omega t) + F_{cutter}\sin(\Omega t) \end{cases} \tag{6}$$

Substituting Equation (6) into Equation (1), Equation (7) can be written as:

$$\begin{cases} \ddot{u}(x,t) = \frac{1}{m_u}\left[m_\mu\Omega^2\varepsilon u(x_u,t)\sin(\Omega t) + F_{cutter}\cos(\Omega t) - c_u\dot{u}(x,t) - k_u u(x,t)\right] \\ \ddot{w}(x,t) = \frac{1}{m_u}\left[m_\mu\Omega^2\varepsilon w(x_u,t)\cos(\Omega t) + F_{cutter}\sin(\Omega t) - c_w\dot{w}(x,t) - k_w w(x,t)\right] \end{cases} \tag{7}$$

The initial values of $u(0)$, $w(0)$, and $\dot{u}(0)$, $\dot{w}(0)$ are assumed as:

$$\begin{cases} u_0 = u(0,0) = 0, w_0 = w(0,0) = 0 \\ \dot{u}_0 = \dot{u}(0,0) = 0, \dot{w}_0 = \dot{w}(0,0) = 0 \end{cases} \tag{8}$$

Assuming that $\dot{u}_0 = p$, $\dot{w}_0 = q$, Equation (7) can be reduced as Equation (9), which are two first-order equations:

$$\begin{cases} \dot{p} = \frac{1}{m_u}\left[m_\mu \Omega^2 \varepsilon u(x_u, t)\sin(\Omega t) + F_{cutter}\cos(\Omega t) - c_u \dot{u}(x,t) - k_u u(x,t)\right] \\ \dot{q} = \frac{1}{m_u}\left[m_\mu \Omega^2 \varepsilon w(x_u, t)\cos(\Omega t) + F_{cutter}\sin(\Omega t) - c_w \dot{w}(x,t) - k_w w(x,t)\right] \end{cases} \tag{9}$$

Equation (9) can be solved by the fourth order of the precision Runge–Kutta numerical integration method based on MATLAB, and the tool tip vibration displacement can be gained.

2.2. Propagation Modelling of Micro-Milling Tool

The typically variable section structure of the micro-milling tool is shown in Figure 2. As Figure 2 shows, there are two parts of the tool: part A includes the blade and the avoided space; part B is the tool arbor, which includes the tapered transition zone and the hilt. Kinetic energy is denoted as T, the potential strain energy is U, and external disturbances are F,

$$T_{tool} = \frac{1}{2}\int_0^L \rho S\left(\dot{u}^2 + \dot{w}^2\right)dx + \frac{1}{2}\int_0^L \rho I\left(\dot{\theta}^2 + \dot{\psi}^2\right)dx + \rho I L \Omega^2 + 2\Omega\int_0^L \rho I \dot{\psi}\theta dx \tag{10}$$

ρ, L, S, and I denote the density length, cross-section, and moment of inertia of the tool. u and w denote the transverse deflections in the y and z directions.

The train energy can be presented as:

$$U_{tool} = \frac{1}{2}\int_0^L EI\left({u_{,xx}}^2 + {w_{,xx}}^2\right)dx + \frac{1}{2}\int_0^L F_{ext}\left({u_{,xx}}^2 + {w_{,xx}}^2\right)dx \tag{11}$$

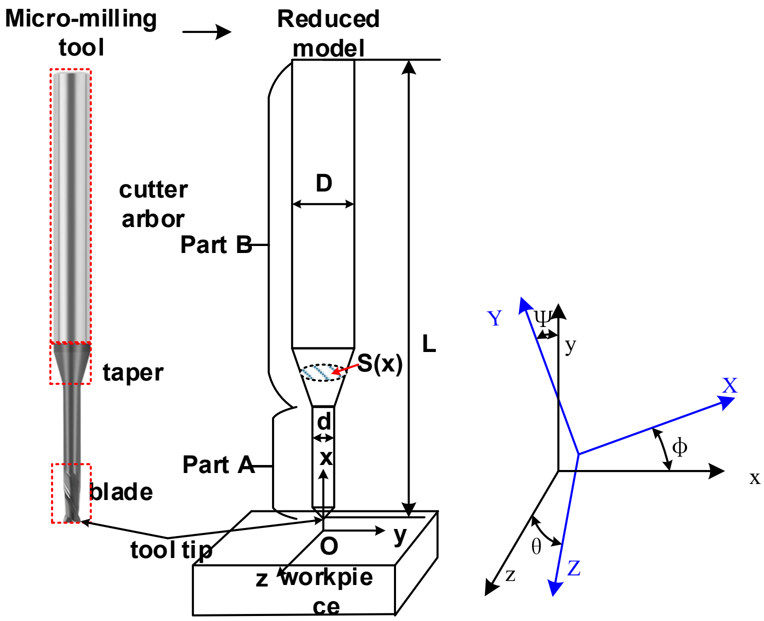

Figure 2. Typical micro-milling tool geometry.

The Lagrange's function of the micro-milling tool horizontal free vibration system is:

$$\begin{cases} \frac{d}{dt}\left(\frac{\partial T_{tool}}{\partial \dot{u}}\right) - \frac{\partial T_{tool}}{\partial u} + \frac{\partial U_{tool}}{\partial u} = 0 \\ \frac{d}{dt}\left(\frac{\partial T_{tool}}{\partial \dot{w}}\right) - \frac{\partial T_{tool}}{\partial w} + \frac{\partial U_{tool}}{\partial w} = 0 \end{cases} \tag{12}$$

Then, substituting Equations (10) and (11) into Equation (12), the motion of the tool system can be written as the following equations:

$$\begin{cases} \rho s(x)\ddot{u}(x,t) - \rho I(x)\Omega\dot{w}(x,t) + d^2/dx^2[EI(x)u_{,xx}(x,t)] = F_u \\ \rho s(x)\ddot{w}(x,t) - \rho I(x)\Omega\dot{u}(x,t) + d^2/dx^2[EI(x)w_{,xx}(x,t)] = F_w \end{cases} \tag{13}$$

Setting

$$\mathrm{W(x,t) = [u(x,t) + jw(x,t)] = U(x)e^{-j\omega t}} \tag{14}$$

Based on Hamilton's principle [27–29], we obtain

$$\rho s(x)\ddot{W} - \rho I(x)\Omega\dot{W} + d^2/dx^2[EI(x)W_{,xx}] = F_{ext} \tag{15}$$

Equation (15) is the kinematic equation of the tool and all the points on the tool satisfy this equation. $y = \begin{pmatrix} u & u_{,x} & Q & M \end{pmatrix}$ is the state vector, where u is the generalized displacement reflecting the general force, $u_{,x}$ is the deflection of the tool at shear stress Q and the bending moment M. Applying the separation principle and matrix transformation over the length of the tool, we have the following transfer representation of the dynamics of the tool:

$$y_L = \left[G(L)e^{\int_0^L A(x)dx}G(0)^{-1}\right]y_0 = \boldsymbol{T}y_0 \tag{16}$$

In Equation (16), $G(0)$ and $G(\mathrm{L})$ are the coordinate transformation matrices when $x = 0$ and $x = L$, respectively.

$$A(x) = \begin{bmatrix} 0 & 1 & 0 & 0 \\ 0 & 0 & 0 & 1 \\ \frac{\rho s(x)(\omega^2+\Omega^2) - j\omega\rho I(x)\Omega}{EI(x)} & 0 & -\frac{2I_{,x}}{I(x)} & -\frac{I_{,xx}}{I(x)} \\ 0 & 0 & 1 & 0 \end{bmatrix} \tag{17}$$

$$G(x) = \begin{bmatrix} 1 & 0 & 0 & 0 \\ 0 & 1 & 0 & 0 \\ 0 & 0 & -EI(x) & 0 \\ 0 & 0 & 1 & EI(x) \end{bmatrix} \tag{18}$$

Substituting (17) and (18) into Equation (16), the transfer matrix T can be gained, and the propagation characteristic of the tool is branded by the eigenvalues of the matrix T. The propagation characteristics of the tool vibration displacement are included in the eigenvalues of the transfer matrix. The eigenvalue λ_i of the transfer matrix is recorded as $\mathrm{e}^{(\alpha_i + \mathrm{j}\beta_i)}$, where α_i is attenuation factor and β_i is the phase angle; when it is not zero, the transmitted signal is attenuated [29].

3. Vibration Characterizes Analysis of the Micro-Milling Tool

3.1. Micro-Milling Tool Parameters

Based on the above models, the vibration propagation characteristics of two micro-milling tools were analyzed. The core geometrical and material parameters of two micro-milling tools are shown in Table 1, and the detailed physical dimension is shown in Figure 3. In order to study the effects of the variable cross-section on tool vibration propagation characteristics, the tools were chosen with the same diameter and size but different cross-sections. The tip radius of Tool A and Tool B are 0.5 µm and 0.2 µm and the blade length of Tool A and Tool B are 3 mm and 1 mm, respectively. Considering that the length of the tool blade is short and the tool tip radius is very small, the tool blades deal with a cone in order to simplify the calculation. It can be seen that in Figure 3, there are two variable-cross-sections of the tools, one part is the tool blade, the other part is the taper between the avoided space and the tool bar. Based on the tool geometry shown in Figure 3, the section area of Tool A and Tool B can be written as Equations (19) and (20), respectively:

$$S_A x = \begin{cases} ae^{bx} & x \in [0,\ 3) \\ \pi {r_{A1}}^2 & x \in [3,\ 18) \\ ce^{dx} & x \in [18,\ 23) \\ \pi {r_{A2}}^2 & x \in [23,\ 50] \end{cases} \tag{19}$$

where $a = \pi {r_{tipA}}^2$, r_{tipA} is the tip radius of Tool A, $b = \frac{1}{3}\log\left(\frac{\pi {r_{A1}}^2}{a}\right)$, $c = \frac{\pi {r_{A1}}^2}{e^{18d}}$, and $d = 0.2\log[(\frac{r_{A2}}{r_{A1}})^2]$.

$$S_B x = \begin{cases} a_1 e^{b_1 x} & x \in [0,\ 1) \\ \pi \cdot {r_{B1}}^2 & x \in [1,\ 5) \\ a_2 e^{b_2 x} & x \in [5,\ 8) \\ a_3 e^{b_3 x} & x \in [8,\ 12) \\ \pi \cdot {r_{B3}}^2 & x \in [12,\ 50) \end{cases} \tag{20}$$

where $a_1 = \pi {r_{tipB}}^2$, r_{tipB} is the tip radius of Tool B, $b_1 = \log\left(\frac{\pi {r_{B1}}^2}{a_1}\right)$, $b_2 = \frac{1}{3}\log\left[\left(\frac{r_{B2}}{r_{B1}}\right)^2\right]$, $a_2 = \frac{\pi \cdot {r_{B1}}^2}{e^{5 \cdot b_2}}$, $a_2 = \frac{\pi \cdot {r_{B2}}^2}{e^{8 \cdot b_3}}$, and $b_3 = \frac{1}{4}\log\left[\left(\frac{r_{B3}}{r_{B2}}\right)^2\right]$.

Table 1. Geometric parameters of Tool A and Tool B.

Micro-End Mill	Tool A	Tool B
Number of tool flutes	2	2
Helix angle	30°	30°
Tool length	50 mm	50 mm
Cutter arbor diameter	4 mm	4 mm
Cutter edge radius	1 mm	0.2 mm
Tool tip radius	0.5 µm	0.2 µm
Cutter edge length	3 mm	1 mm
Geometric shapes	Spiral conical double edge	Spiral conical double edge
Material	Cemented carbide	Cemented carbide
Coating material	Tungsten steel	Tungsten steel
Density/(kg·m^{-3})	15,000	15,000
Elasticity modulus/GPa	600	600
Poisson's ratio	0.22	0.22

Poisson's ratio 0.22 0.22

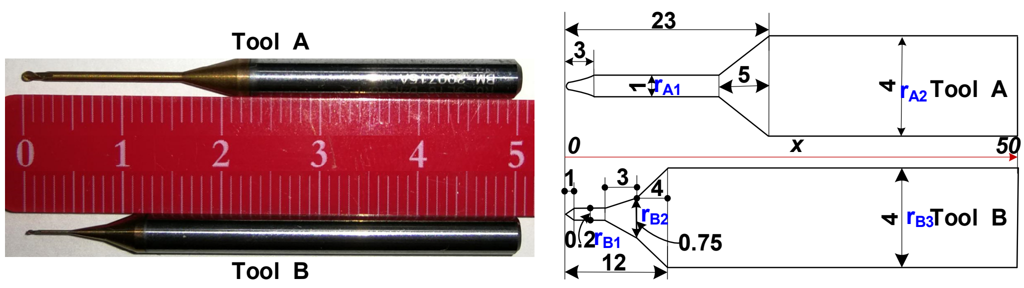

Figure 3. Geometrical parameters of micro-milling Tool A and micro-milling Tool B.

3.2. Micro-Milling Tool Vibration Propagation Characteristic

The parameters of the two tools shown in the Figure 3 were substituted into Equations (19) and (20), then by solving Equation (16), the eigenvalues of the transfer matrix in the equation can be obtained with the help of the MATLAB numerical calculation tool. The normalized vibration amplitude attenuation factor of Tool A and Tool B is shown in Figure 4. It can be seen that there are two attenuation bands of Tool A and Tool B, respectively. The locations of the tool attenuation band are mainly distributed at the variable section of the tools. However, the stopband characteristics of two tools are significantly different to each other as the section length and the section area ratio vary. The major stopbands are located at sections 0 to 3 mm and sections 17 mm to 23 mm of Tool A. The major stopbands are located at sections 0 to 1 mm and sections 5 mm to 12 mm of Tool B. It can be seen that the most dramatic part of the attenuation factor is on the tool tip, which means that a significant part of the vibration signal may be lost when the vibration information transfers from tool tip to tool bar. The taper part is another important point for stopping vibration transmission, and the distribution of the attenuation factor of Tool B is markedly different from Tool A because it consists of two cones of variable cross-sections, which can be seen in Figure 3.

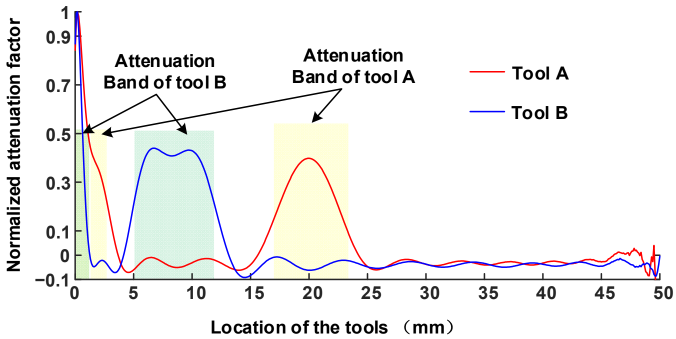

Figure 4. Normalized vibration amplitude attenuation factors of Tool A and Tool B.

The normalized frequency attenuation factor of Tool A and Tool B is shown in Figure 5. The micro-milling tools are more like low pass filters, as Figure 5 shows. However, the attenuation factors are small at low frequencies and large at high frequencies. For bigger attenuation factors, it can be treated as a stopband of the tool. As Figure 5 shows that the cut-off frequencies of Tool A and Tool B are 8.5 KHz and 9.4 KHz, respectively. Usually, the spindle speed in the micro-milling process is above 50,000 RPM. Taking a 4-blade micro-milling tool with 150,000 RPM as an example, the contact frequency between tool tip and workpiece is 10 KHz, which is at the tool cutoff frequency.

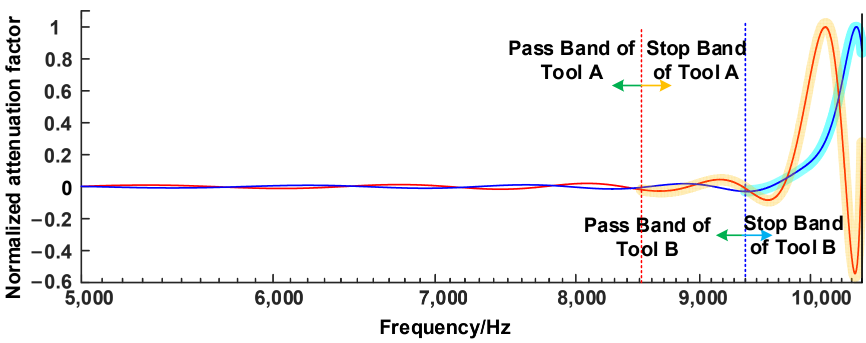

Figure 5. Normalized frequency attenuation factor of Tool A and Tool B.

When comparing Figures 4 and 5, it can be seen that the resistance of the micro-milling tool to vibration signal transmission is closely related to its structure. The whole tool is similar to a low-pass filter. In order to study the vibration of the tool at different positions, a simulation was carried out, and its results are shown in Figures 6–9. Based on Equation (9), by the fourth order of precision Runge–Kutta numerical integration method based on MATLAB, the response of the tip of Tool A and Tool B with an impact force of 1N are gained, as seen Figures 6 and 8. Compared with Figures 6 and 8, it can be seen that the vibration decay rates are different due to the differing cross-sections of Tool A and Tool B, the vibration amplitude attenuation speed of Tool B is faster than that of the Tool A. In contrast, the time domain and frequency domain transfer characteristics of Tool A are shown in Figure 7. As Figure 7a shows, the vibration amplitude of the tool tip is nearly 67 times that of the tool bar. Figure 7b shows the frequency domain transfer characteristics of Tool A, it can be seen that the resonance frequencies of Tool A are mainly concentrated at 10 kHz and 17 kHz. Furthermore, the tool vibration frequency information dissipates rapidly with the change of its cross section area. The time domain and frequency domain transfer characteristics of Tool B is shown in Figure 9. Compared to Tool A, which is even more remarkable, the vibration amplitude of the tool tip is nearly 250 times that of the tool bar, which shows the vibration propagation of Tool B in Figure 9a. However, due to the smaller front end size of Tool B, it has more complex resonance frequencies. It can be seen that the resonance frequencies of Tool B are mainly concentrated at 10 kHz, 18 kHz, and 27 kHz. Furthermore, because the variable section is mainly concentrated at the front of the Tool B, the vibration information of the tool tip decays rapidly at this stage, as shown in Figure 9b. Based on the simulation results in Figures 7 and 9, this means that in the high-speed micro-milling process, the farther away from the tool tip, the more difficult to capture the key information of micro-milling tool vibration.

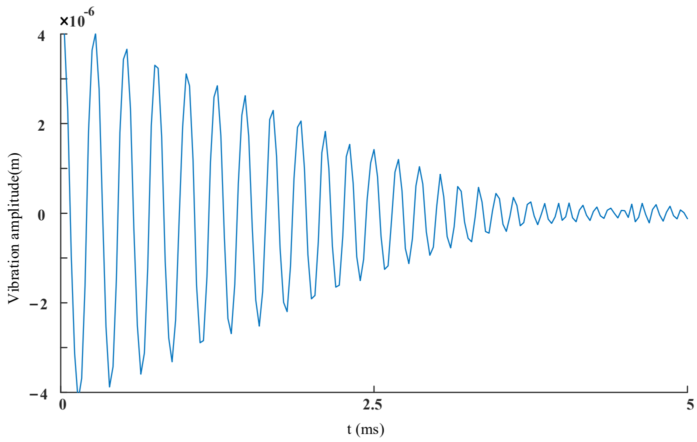

Figure 6. Impact response of the tip of Tool A.

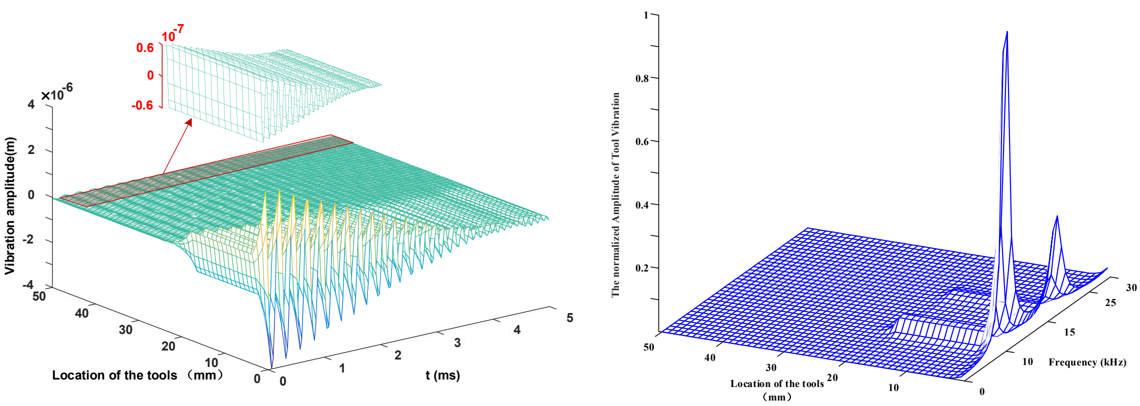

(**a**) (**b**)

Figure 7. Vibration Propagation of Tool A. (**a**) Time domain transfer characteristic and (**b**) frequency domain transfer characteristics.

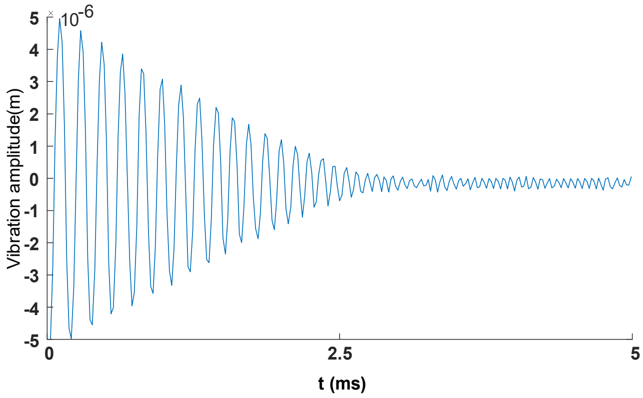

Figure 8. Impact response of the tip of Tool B.

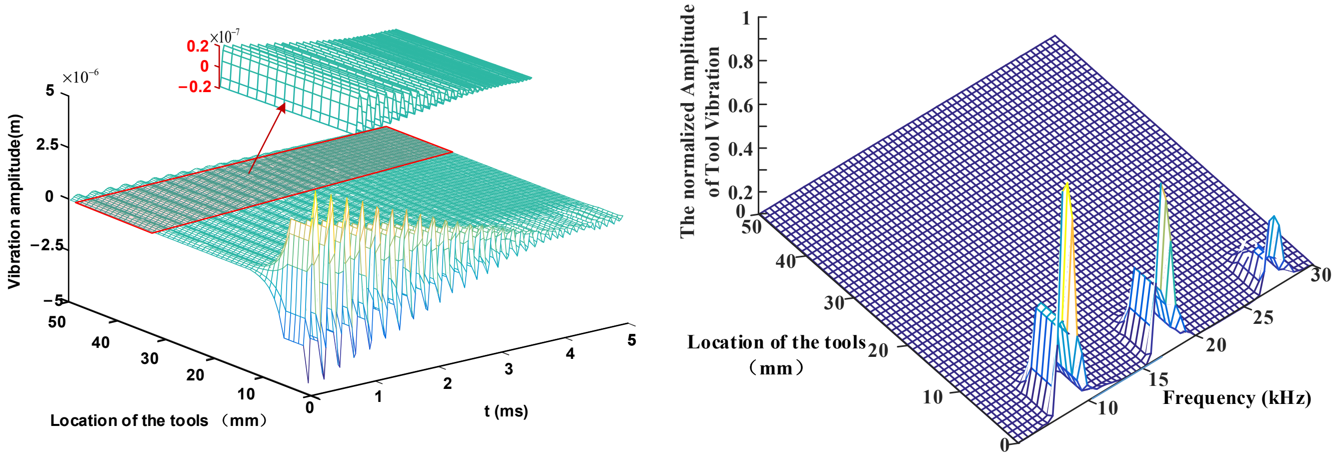

Figure 9. Vibration Propagation of Tool B. (**a**) Time domain transfer characteristic and (**b**) frequency domain transfer characteristics.

4. Experiment Results and Discussions

Figure 10 shows the micro-milling tool vibration measurement experimental system. It consists of seven main parts: a desktop milling machine (with micro-milling tool), a voltage-stabilized source, four light sources, an optical-electric conversion module, a DAQ card, and the optical fiber sensor array. The speed range of the desktop milling machines is from 0 to 10,000 RPM with the power of 480 W. It is made by the MENCHAO Company. The optical fiber sensor array consists of four optical fiber displacement sensors. The sensor [30] was developed by the author with a measurement range of 2 mm and the sensitivity of 2.668 mv/µm. The maximum signal frequency of the sensor system designed by us is 50 kHz, its linear error is 0.12% with the max measurement uncertainty of 2.4 µm. The wavelength and power of the light source are 650 nm and 10 mW, respectively. An OPT01 chip is used in photoelectric conversion module, and its output voltage is approximately 0.45 V/µw at a 650 nm wavelength. The DAQ card USB-1901 made by ADLINK was chosen, which, with a maximum sampling rate of 250 kS/s USB 2.0-based high-performance DAQ modules, allows four different voltage input ranges.

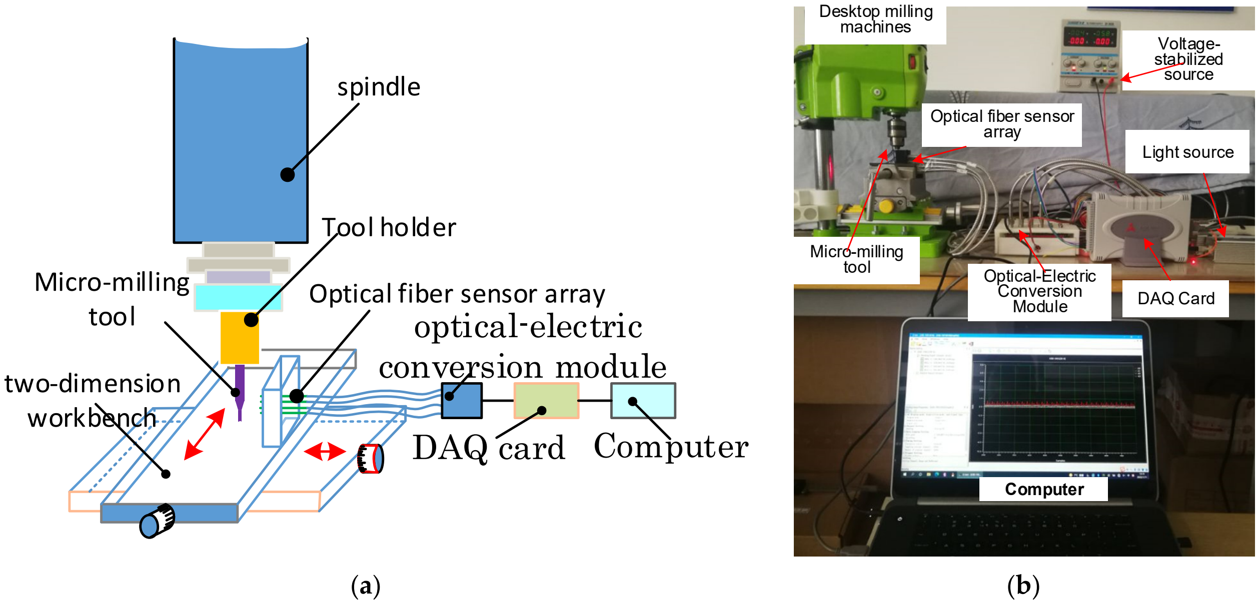

Figure 10. Micro-milling tool vibration measurement experimental system set up. (**a**) Schematic diagram of the set-up and (**b**) the actual set up for micro-milling tool.

The relative position of the sensor array and Tool A and Tool B is shown in Figure 11. Sensor 1 is used for measuring the vibration displacement of the tool tip. Sensor 2, sensor 3, and sensor 4 are used to measure the vibration of the Tool A at 10 mm, 18 mm, and 24 mm, respectively, from the tool tip. Due to the limitations of Tool B and the size of the sensors, the vibration measurement points of Tool B of sensor 2, sensor 3, and sensor 4 are located at 8 mm, 20 mm, and 30 mm from the tool tip, respectively. In fact, in the machining process, the tool holder is the key interface connecting the tool and the machine tool. For example, the clamping rotary accuracy determines the dimensional accuracy of the workpiece and the vibration damping characteristics of the tool handle have a decisive impact on the service life of the tool and the installation error and runout of the tool on the tool handle also have a non-negligible impact on the tool vibration. However, considering the size of the micro-milling tool is very small compared with the tool holder, the vibration signal of the micro-milling tool is extremely weak, so the sensor layout is mainly extant around the tool.

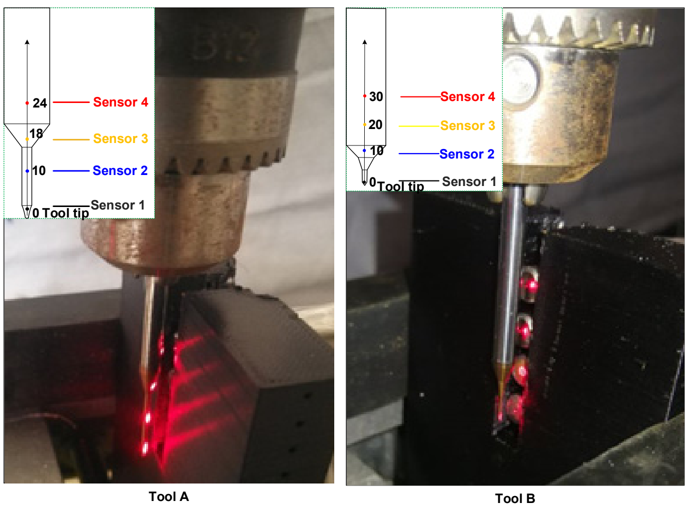

Figure 11. The relative position of sensor array and the tool.

In the experiments, one end of a very fine steel wire (diameter of 0.1 mm, 304 stainless steel) was hung on the tip of the tool, and the other end was fixed on a constant force spring sheet. The length of the constant force spring was adjusted. When the tension reached 4 N, the steel wire was cut quickly, and a transient force of 4 N was applied to the tip. Ten measurements per position were carried out. The impact vibration displacement response of Tool A is shown in Figure 12. Figure 12a shows the raw data of the impact response of Tool A in 5 ms, and the signal variation trend measured by sensor 1 agrees with the curve in Figure 6. In the meantime, the vibration displacement signal measured by sensor 2, sensor 3, and sensor 4 decreases with the distance far away from the tip of Tool A, which is obvious. In order to show the difference between the signals of each sensor more clearly, Figure 12b shows the first 0.5 ms impulse response signal (the signal is de-noised by the wavelet, using MATLAB toolbox). The proportion of vibration attenuation varies greatly compared with measurement point 1 (signal of sensor 1), measurement point 2 (signal of sensor 2), measurement point 3 (signal of sensor 3), and measurement point 4 (signal of sensor 4). The max vibration displacement of measurement point 1 is about 3.5 times measurement point 2, but nearly 18 times measurement point 3. Furthermore, the periodic vibration of measurement point 1 and measurement point 2 are highly similar; the vibration waveforms of measurement 3 and measurement 4 are obviously different to measurement point 1 and measurement point 2, based the time domain signals shown in Figure 12. This result corresponds well with the simulation conclusion in Figure 7a.

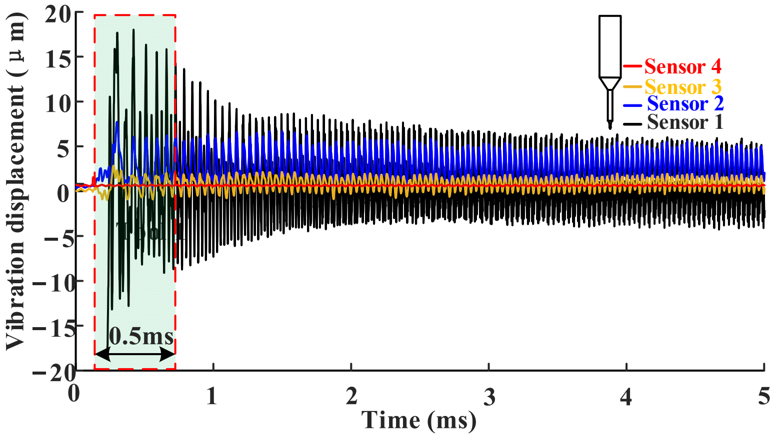

(**a**)

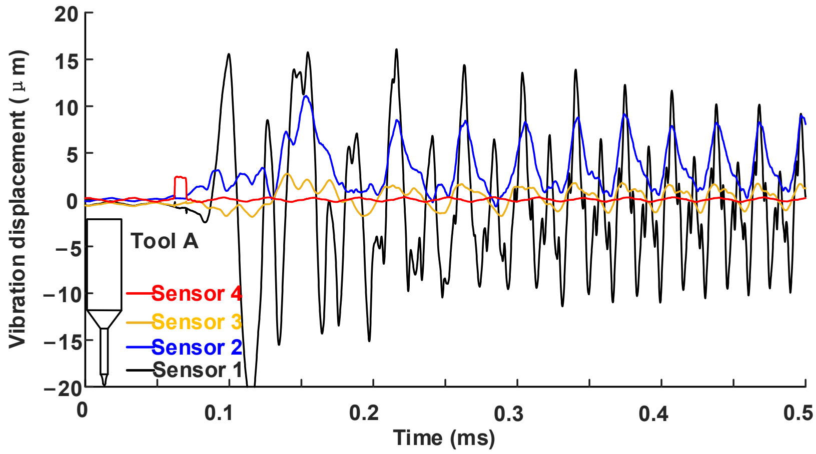

(**b**)

Figure 12. Impact response of Tool A at different positions. (**a**) Impact response of Tool A (raw data), (**b**) De-noised data (for clearer expression, only the first 0.5 ms is given here).

Figure 13 shows the frequency propagation of Tool A. Based on spectrum analysis of the received impact response signals of measurement point 1, point 2, point 3, and point 4 (corresponding to sensor 1 sensor 2, sensor 3, and sensor 4, respectively), it can be seen that there are two resonant frequencies of Tool A based on the signal received by sensor 1 (according to measurement point 1), 11.2 kHZ and 16.8 kHz. However, with the measurement points far away from the tool tip, the intensity of the signal with frequency of 11.2 kHz weakened. The 16.8 kHz signal suddenly disappeared at measurement point 2, measurement point 3, and measurement point 4. The spectrum analysis result of signal 4 (based on sensor 4) is more prominent, no distinct resonant frequencies appear in the signal.

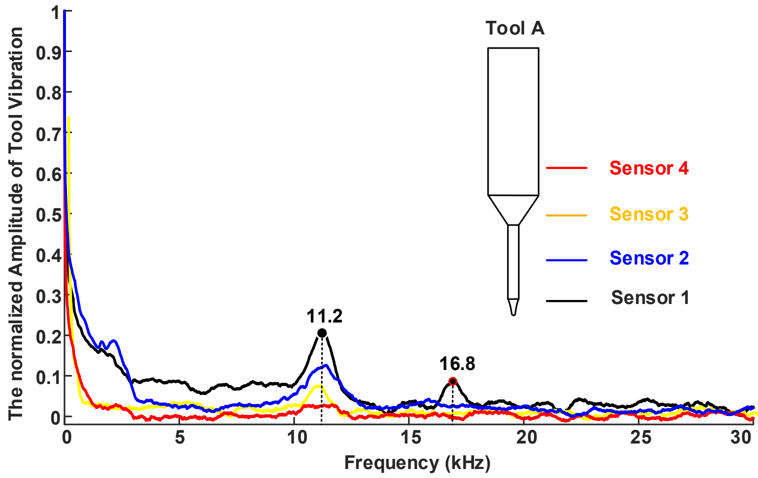

Figure 13. Frequency propagation of Tool A based on impact response.

Compared with the frequency propagation curves in Figure 13 and the vibration displacement curves in Figure 12, most information components are in measuring point 1. Although the same cross-section and similar signal waveforms are extant in the time domains of measurement point 1 and point 2, high frequency information is rapidly dissipated, moving from the tool tip to measuring point 2. It can be seen that this result is well consistent with the tool vibration information transmission characteristics in Figures 4 and 5. Meanwhile, it can be seen that the high frequency vibration information of the tool tip is first prevented from propagating along the tool, as a large proportion of the tip area changes. However, the low-frequency vibration information of the tool dissipates relatively slowly in the propagation. Comparing with the results in Figures 13 and 7b, it can be seen that the variation of the tool cross-section area not only affects the attenuation speed of the vibration signal amplitude but also has an obvious influence on the dissipation speed of the vibration signal frequency.

Figure 14 shows the impact response of Tool B at different positions. Figure 14a shows the raw data of the impact response of Tool B in 5 ms, and Figure 14b shows the first 0.5 ms impulse response signal (the signal is de-noised by the wavelet, using the MATLAB toolbox). The maximum vibration displacement of measurement point 1 is about 45 μm. However, the maximum vibration displacement of measurement point 2 is about 4 μm, and the overall intensity of the signal is relatively weak. The signal strength of measurement point 3 and point 4 are too weak to compare and analyze. Compared to Figure 12, the influence of tool geometric shape is particularly significant. Compared with the distribution characteristics of the vibration attenuation factors of two micro-milling tools shown in Figure 4, it can be seen that the variation of tool cross section area directly affects the vibration attenuation factor distribution, which leads to the transmission efficiency of tool vibration amplitude signal in the tool. This result agrees with the simulation conclusion in Figure 9a.

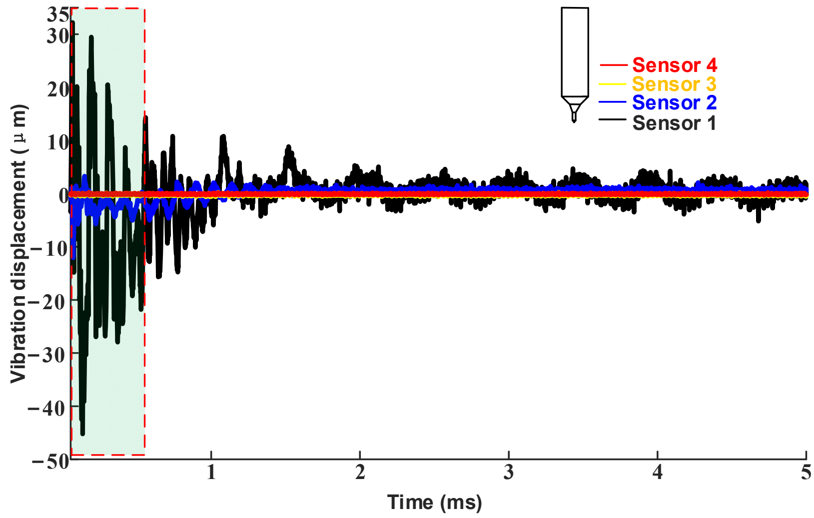

(**a**)

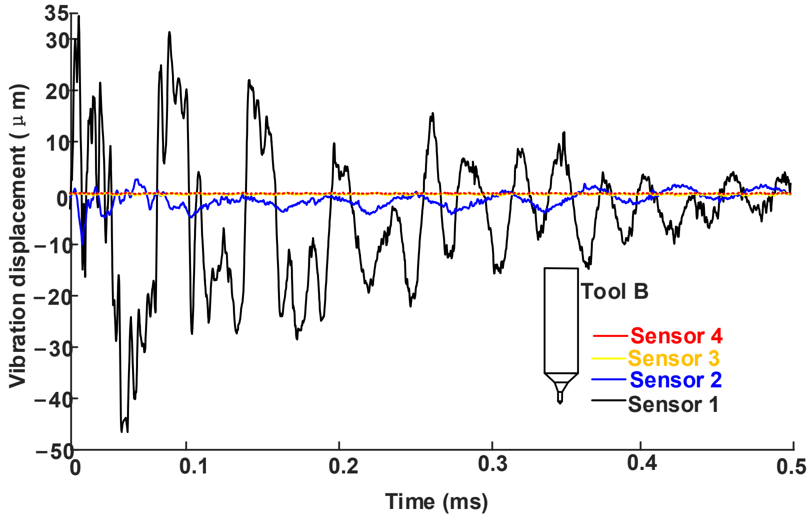

(**b**)

Figure 14. Impact response of Tool B at different positions. (**a**) raw data and (**b**) de-noised data (for clearer expression, only the first 0.5 ms is given here).

Figure 15 shows the frequency propagation curves of Tool B based on impact response. Differently to Tool A, as can be seen in Figure 13, there are three resonant frequencies of the tool based on the signal of measurement point 1 (sensor 1). They are 10.2 kHz, 17.6 kHz, and 26.7 Hz, respectively. On the other hand, the intensity of the signal based on sensor 2 (according to measurement point 2) is obviously weakened, which just leaves the frequency of 10.2 kHz and 17.6 kHz. The 26.7 kHz signal disappeared at measurement point 2. There are no distinct resonant frequencies that appear based on the spectrum analysis results of signal 3 (based on sensor 3 according to measurement point 3) and signal 4 (based on sensor 4 according to measurement 4) in Figure 15. The information dissipates rapidly with the measurement points far away from the tip of Tool B. This means that the vibration displacement sensor must be placed as close to the tip as it can be, especially for micro-milling tools with large cross-sections. Compared to the results in Figures 9b and 15 , it can be seen that the amplitude and frequency of the vibration signal is mainly dissipated in the variable cross-section part of Tool B.

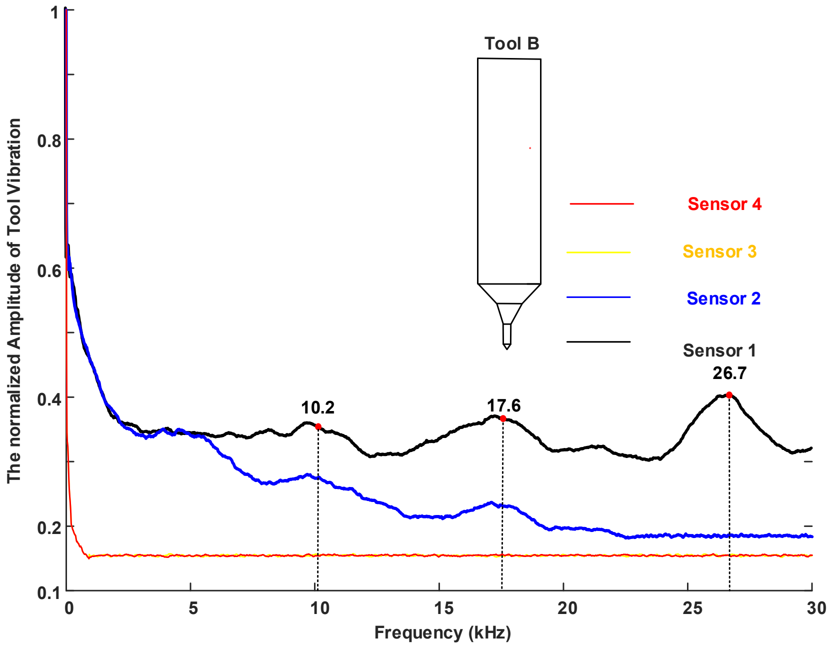

Figure 15. Frequency propagation of Tool B based on impact response.

Comparing the time domain and frequency domain curves of Tool A and Tool B in Figures 12–15, it can be seen that the vibration information propagation characteristics in the tool have obvious differences according to tool geometry. Figure 16 shows the cross-section areas of Tool A and Tool B. As there are two parts of the cross-section of Tool A, the dissipative vibration process is mainly accomplished in two steps. Figures 17 and 18 show the vibration propagation curves of Tool A and Tool B in the start–stop process. In Tool A, the start–stop process lasted for 5 s, then the tool speed was accelerated to 10,000 RPM in 1 s, was held for 2 s, and then slowed to 0 RPM in 2 s. In Tool B, the tool speed was accelerated to 10,000 RPM in 1 s, was held for 3 s, and then slowed to 0 RPM in 1 s. As Figures 17 and 18 show, the attenuation of vibration displacement has a certain correlation with the change of tool section area. For Tool A, in the uniform rotation process, the vibration displacement of measuring point 1 is 7.3 μm, which is about 3.2 times the measurement of point 2. In fact, it is very difficult to measure the real tool tip vibration as its too small to find the correct measurement tool, so measuring point 1 actually has a certain distance of about 2.8 mm from the tool tip. The ratio of the cross-section of measurement point 2 and measurement point 1 is 4.5 and 3.2 divided by cross-section ratio 4.5 is 0.71. The vibration displacement of measuring point 2 is 6.2 times measurement point 3; however, the ratio of the cross-section of measurement point 3 and measurement point 2 is 16. Here, 6.2 divided by the cross-section ratio 16 is 0.39. For Tool B, the vibration displacement of measuring point 1 is 11.6 μm in the uniform rotation process, and it is about 38.7 times the measurement of point 2. The ratio of cross-section of measurement point 2 and measurement point 1 is 49.17, which can be calculated based on Figure 16. Then, 38.7 divided by the cross-section ratio 49.17 is 0.79. Compared with Tool A, Tool B has a smaller geometry and a larger decay rate of the vibration amplitude. In contrast with the above results, it can be seen that a bigger ratio of the cross-section has a bigger attenuation of the vibration amplitude but a smaller geometry with a bigger decay rate of the vibration amplitude. Where the tool cross section area changes sharply, the tool vibration signal decreases faster with transmission and the high-frequency information dissipation speed is more obvious.

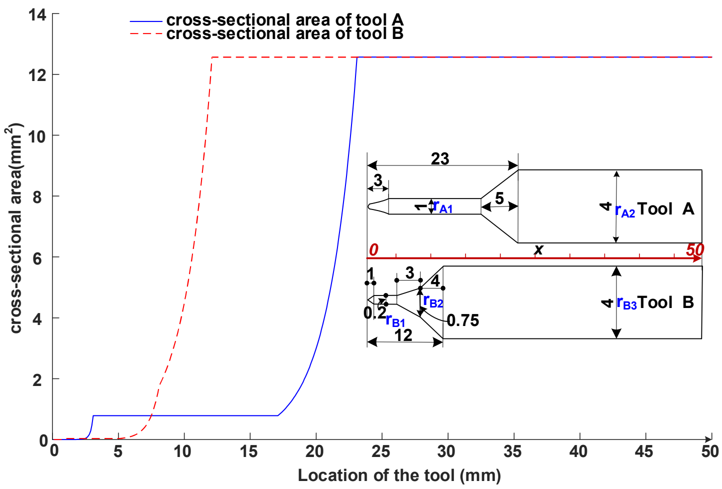

Figure 16. Cross-section area of Tool A and Tool B.

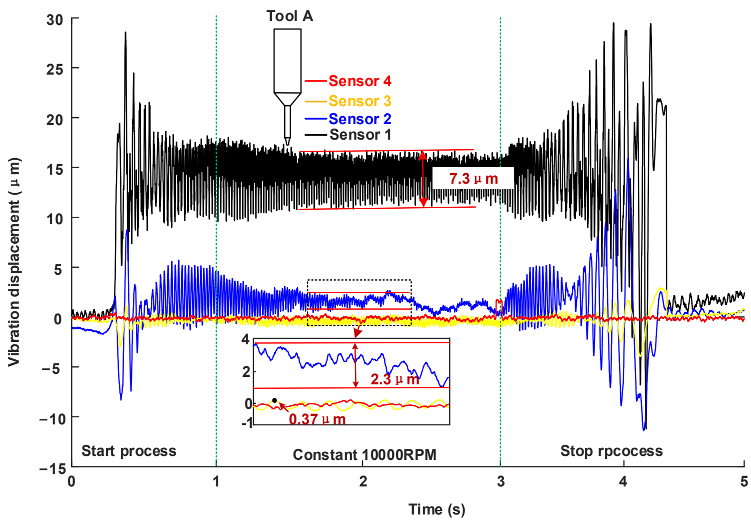

Figure 17. Vibration propagation of Tool A in the start–stop process.

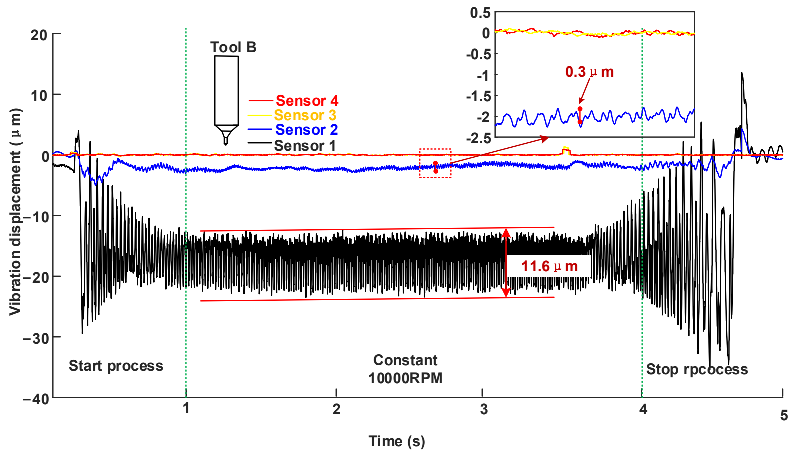

Figure 18. Vibration propagation of Tool B in start–stop process.

The above results show that the variation of tool cross section area has a significant effect on tool vibration transmission. Compared with the force dynamometer, the displacement sensor is more capable of chatter detection in high-speed micro-milling [31]. However, without considering tool vibration transmission characteristics, a laser displacement sensor was mounted for tool bar vibration measurement and only the low-frequency information of tool vibration is obtained [31]. To further demonstrate the results of this paper, we compared the experimental results with those of Reference [32]. In order to analyze the device developed to perform the experimental modal analysis of micro-milling tools, impact tests of a cylindrical dummy tool and two micro-milling tools with different diameters (0.2 mm and 1 mm, respectively) were carried out to demonstrate the device application of Crichigno Filho, J.M. [32]. The results of experimental FRF receptance and coherence are shown in Figure 19. For the dummy tool, in Figure 19a, although the signal intensity is attenuated, the information dissipation is not obvious. By contrast, in Figure 19b, the consistency of vibration signal and excitation is obviously different at different positions of the tool. Which means that information dissipation occurs in the cutting tool during the transmission of the vibration signal. Although the structural parameters and excitation positions are different, this result still confirms the conclusion of this paper to some extent.

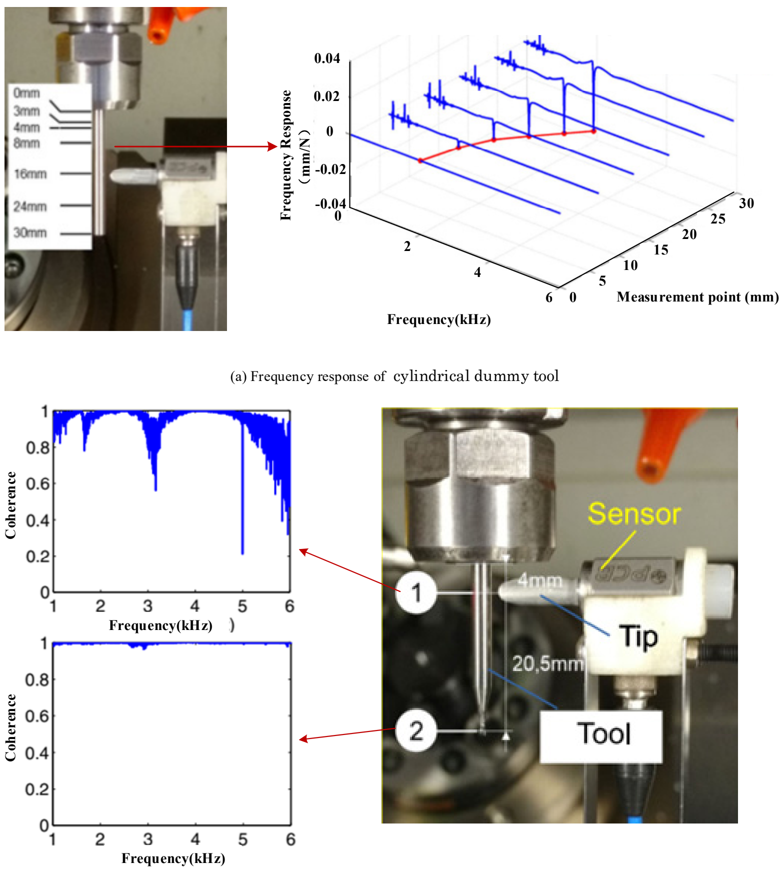

(a) Frequency response of cylindrical dummy tool

(b) The coherence between signal and excitation force at different positions of tool (1 mm tool diameter)

Figure 19. Tool vibration responses with different structure [32].

5. Conclusions

Focusing on the problem of micro-milling tool vibration propagation, a vibration propagation model was built for the micro end milling process. The vibration amplitude and frequency transfer characteristics of two typical micro-milling tools were analyzed. The simulation results show that the locations of the tool attenuation band are mainly distributed at the variable section of the tools. However, the stopband characteristics of two tools are significantly different from each other, as the section length and the section area ratio vary. A micro-milling tool vibration measurement experimental system was set up to test the above model. Pulse impact measurement experiments and start–stop vibration measurement experiments were carried out for Tool A and Tool B, respectively. The results show that a bigger ratio of the cross-section has a larger attenuation to vibration amplitude;

meanwhile, smaller geometry with a bigger decay rate of vibration amplitude. However, limited by the small size of the micro-milling tool and the space for sensor placement, it is difficult to obtain the vibration data for the whole tool. In spite of this, the results of this paper still have reference significance: the information dissipates rapidly with the measurement points far away from the tip of the micro-milling tool. This means that the vibration displacement sensor must be placed as close to the tip as it can be, especially for micro-milling tools with large cross-sections.

The possible industrial applications for this research mainly include two aspects: (1) it provides a reference for tool geometry design, since the variation of cross-section area directly affects the transmission and the dissipation of tool vibration information, and (2) to guide the design and application of micro-milling tool vibration measurement sensors, because the complexity of the micro-milling tool structure and the precision of the cutting process makes it is very important to design a sensor and a detection system suitable for weak information acquisition [33]. However, there are still some problems to be solved in the future, such as the effect of a tool holder, the machine parameters, and workpiece material on tool vibration. It is important to point out that micro-milling tools have typical characteristics of weak rigidity, and their vibrations include transverse vibration, longitudinal vibration, and torsional vibrations. The movement is a spatial concept. In this paper, only the transverse vibration propagation characteristics of the micro-milling tool were studied. In future research, the vibration propagation characteristics of the micro-milling tool will be analyzed from the perspective of three-dimensional space. Therefore, it will include two key issues: the first is to shed new light on the transmission and dissipation law of micro-milling tool vibration from an informatics perspective and establish a mathematical model that can unify physical tool structure, energy transfer, and information expression. The second is the dynamic precision measurement of the vibration hologram in the process of the micro-cutting tool, observing the spatial vibration pattern of micro-milling tool tip precisely.

Funding: This research was funded by Innovation fund of Nanjing Institute of Technology, grant number CKJA201801.

Conflicts of Interest: The author declares that they have no conflict of interest.

References

1. Câmara, M.A.; Rubio, J.C.C.; Abrão, A.M.; Davim, J.P. State of the Art on Micro milling of Materials, a Review. *J. Mater. Sci. Technol.* **2012**, *28*, 673–685. [CrossRef]
2. O'Toole, L.; Kang, C.-W.; Fang, F.-Z. Precision micro-milling process: State of the art. *Adv. Manuf.* **2021**, *9*, 173–205. [CrossRef] [PubMed]
3. Balázs, B.Z.; Geier, N.; Takács, M.; Davim, J.P. A review on micro-milling: Recent advances and future trends. *Int. J. Adv. Manuf. Technol.* **2021**, *112*, 655–684. [CrossRef]
4. Mokhtari, A.; Jalili, M.M.; Mazidi, A.; Abootorabi, M.M. Size dependent vibration analysis of micro-milling operations with process damping and structural nonlinearities. *Eur. J. Mech. A Solids* **2019**, *76*, 57–69. [CrossRef]
5. Farhadmanesh, M.; Ahmadi, K. Online identification of mechanistic milling force models. *Mech. Syst. Signal Process.* **2021**, *149*, 107318. [CrossRef]
6. Shakeri, S.; Samani, F.S. Application of linear and nonlinear vibration absorbers in micro-milling process in order to suppress regenerative chatter. *Nonlinear Dyn.* **2017**, *89*, 851–862. [CrossRef]
7. Li, H.; Jing, X.; Wang, J. Detection and analysis of chatter occurrence in micro-milling process. *Proc. Inst. Mech. Eng. Part B J. Eng. Manuf.* **2014**, *228*, 1359–1371. [CrossRef]
8. Chen, W.; Teng, X.; Huo, D.; Wang, Q. An improved cutting force model for micro milling considering machining dynamics. *Int. J. Adv. Manuf. Technol.* **2017**, *93*, 3005–3016. [CrossRef]
9. David, C.; Sagris, D.; Stergianni, E.; Tsiafis, C.; Tsiafis, I. Experimental Analysis of the Effect of Vibration Phenomena on Workpiece Topomorphy Due to Cutter Runout in End-Milling Process. *Machines* **2018**, *6*, 27. [CrossRef]
10. Mustapha, K.B.; Zhong, Z.W. A hybrid analytical model for the transverse vibration response of a micro-end mill. *Mech. Syst. Signal Process.* **2013**, *34*, 321–339. [CrossRef]
11. Du, Y.; Song, Q.; Liu, Z.; Wang, Z.; Wan, Y. Size-dependent responses of micro-end mill based on strain gradient elasticity theory. *Int. J. Adv. Manuf. Technol.* **2019**, *100*, 1839–1854. [CrossRef]

12. Lu, X.; Zhang, H.; Jia, Z.; Feng, Y.; Liang, S.Y. Floor surface roughness model considering tool vibration in the process of micro-milling. *Int. J. Adv. Manuf. Technol.* **2017**, *94*, 4415–4425. [CrossRef]
13. Lu, X.; Jia, Z.; Liu, S.; Yang, K.; Feng, Y.; Liang, S.Y. Chatter Stability of Micro-Milling by Considering the Centrifugal Force and Gyroscopic Effect of the Spindle. *J. Manuf. Sci. Eng.* **2019**, *141*, 111003. [CrossRef]
14. Lu, X.; Jia, Z.; Wang, X.; Liu, Y.; Liu, M.; Feng, Y.; Liang, S.Y. Measurement and prediction of vibration displacement in micro-milling of nickel-based superalloy. *Measurement* **2019**, *145*, 254–263. [CrossRef]
15. Tsai, N.-C.; Chen, D.-C.; Lee, R.-M. Chatter prevention for milling process by acoustic signal feedback. *Int. J. Adv. Manuf. Technol.* **2009**, *47*, 1013–1021. [CrossRef]
16. Ray, D.; Puri, A.B.; Hanumaiah, N.; Halder, S. Analysis on specific cutting energy in micro milling of bulk metallic glass. *Int. J. Adv. Manuf. Technol.* **2020**, *108*, 245–261. [CrossRef]
17. Ding, P.; Huang, X.; Zhang, X.; Wang, C.; Gao, T.; Chang, M.; Li, Y. Reliability updating and parameter inversion of micro-milling. *Mech. Syst. Signal Process.* **2022**, *174*, 109105. [CrossRef]
18. Wang, R.; Song, Q.; Liu, Z.; Ma, H.; Liu, Z. Multi-condition identification in milling Ti-6Al-4V thin-walled parts based on sensor fusion. *Mech. Syst. Signal Process.* **2021**, *164*, 108264. [CrossRef]
19. Zhou, Y.; Xue, W. A Multisensor Fusion Method for Tool Condition Monitoring in Milling. *Sensors* **2018**, *18*, 3866. [CrossRef]
20. Polli, M.L.; Weingaertner, W.L.; Schroeter, R.B.; Gomes, J.D.O. Analysis of high-speed milling dynamic stability through sound pressure, machining force and tool displacement measurements. *Proc. Inst. Mech. Eng. Part B J. Eng. Manuf.* **2012**, *226*, 1774–1783. [CrossRef]
21. Jiao, X.J.; Ma, J.M. The Analysis of Longitudinal Impact Response for Variable Cross-Section Rod. *Key Eng. Mater.* **2016**, *693*, 504–510. [CrossRef]
22. Chen, R.; Hu, C.; Xu, J.; Gong, Z.; Liu, L.; Wang, P.; Chen, X. Research on guided wave propagation characteristics in turnout rails with variable cross-section. *J. Sound Vib.* **2020**, *494*, 115853. [CrossRef]
23. Khodabakhshpour-Bariki, S.; Jafari-Talookolaei, R.A.; Attar, M.; Eyvazian, A. Free vibration analysis of composite curved beams with stepped cross-section. *Structures* **2021**, *33*, 4828–4842. [CrossRef]
24. Mamedov, A. Micro milling process modeling: A review. *Manuf. Rev.* **2021**, *8*, 3. [CrossRef]
25. Zhu, Z.; Peng, B.; Feng, R.; Wang, L.; Jiao, S.; Dong, Y. Molecular dynamics simulation of chip formation mechanism in single-crystal nickel nanomachining. *Sci. China Technol. Sci.* **2019**, *62*, 1916–1926. [CrossRef]
26. Xuewei, Z.; Tianbiao, Y.; Wanshan, W. Chatter stability of micro end milling by considering process nonlinearities and process damping. *Int. J. Adv. Manuf. Technol.* **2016**, *87*, 2785–2796.
27. Gan, C.; Wei, Y.; Yang, S. Longitudinal wave propagation in a rod with variable cross-section. *J. Sound Vib.* **2014**, *333*, 434–445. [CrossRef]
28. Gan, C.; Wei, Y.; Yang, S. Longitudinal wave propagation in a multi-step rod with variable cross-section. *J. Vib. Control* **2016**, *22*, 837–852. [CrossRef]
29. Wei, Y.; Pan, J.; Yang, S. Experimental Study about the Propagation Characteristics of the Elastic Wave in Rod with Non-uniform Cross-section. *J. Mech. Eng.* **2020**, *56*, 258–264.
30. Jia, B.; Yu, J. A Differential Light Intensity-Modulation Optical Fiber Bundles Designed for Milling Tool Vibration Measurement. *IEEE Access* **2021**, *9*, 84799–84810. [CrossRef]
31. Singh, K.K.; Singh, R.; Kartik, V. Comparative Study of Chatter Detection Methods for High-Speed Micromilling of Ti6Al4V. *Procedia Manuf.* **2015**, *1*, 593–606. [CrossRef]
32. Filho, J.M.C.; Melotti, S. Evaluation of an experimental modal analysis device for micromilling tools. *Int. J. Adv. Manuf. Technol.* **2022**, *119*, 6679–6692. [CrossRef]
33. Chen, N.; Li, H.N.; Wu, J.; Li, Z.; Li, L.; Liu, G.; He, N. Advances in micro milling: From tool fabrication to process outcomes. *Int. J. Mach. Tools Manuf.* **2020**, *160*, 103670. [CrossRef]